Spin-orbit coupling and anisotropic exchange in two-electron double quantum dots

Fabio Baruffa,[1] Peter Stano,[2,3] and Jaroslav Fabian[1]
[1]*Institute for Theoretical Physics, University of Regensburg, 93040 Regensburg, Germany*
[2]*Institute of Physics, Slovak Academy of Sciences, Bratislava 845 11, Slovakia*
[3]*Physics Department, University of Arizona, 1118 East 4th Street, Tucson, Arizona 85721, USA*
(Received 15 April 2010; revised manuscript received 25 June 2010; published 21 July 2010)

The influence of the spin-orbit interactions on the energy spectrum of two-electron laterally coupled quantum dots is investigated. The effective Hamiltonian for a spin qubit pair proposed in Baruffa *et al.* [Phys. Rev. Lett. **104**, 126401 (2010)] is confronted with exact numerical results in single and double quantum dots in zero and finite magnetic field. The anisotropic exchange Hamiltonian is found quantitatively reliable in double dots in general. There are two findings of particular practical importance: (i) the model stays valid even for maximal possible interdot coupling (a single dot), due to the absence of a coupling to the nearest excited level, a fact following from the dot symmetry. (ii) In a weak-coupling regime, the Heitler-London approximation gives quantitatively correct anisotropic exchange parameters even in a finite magnetic field, although this method is known to fail for the isotropic exchange. The small discrepancy between the analytical model (which employs the linear Dresselhaus and Bychkov-Rashba spin-orbit terms) and the numerical data for GaAs quantum dots is found to be mostly due to the cubic Dresselhaus term.

DOI: 10.1103/PhysRevB.82.045311 PACS number(s): 71.70.Gm, 71.70.Ej, 73.21.La, 75.30.Et

I. INTRODUCTION

The lowest singlet and triplet states of a two-electron system are split by the exchange energy. This is a direct consequence of the Pauli exclusion principle and the Coulomb interaction. As a result, a spin structure may appear even without explicit spin dependent interactions.[1]

In quantum dot spin qubits[2] the exchange interaction implements a fundamental two-qubit gate.[3,4] Compared to single qubit gates,[5,6] the exchange-based gates are much faster[7] and easier to control locally, motivating the solely exchange-based quantum computation.[8] The control is based on the exponential sensitivity of the exchange energy on the interparticle distance. Manipulation then can proceed, for example, by shifting the single-particle states electrically[7,9,10] or compressing them magnetically.[11]

The practical manipulation schemes require quantitative knowledge of the exchange energy. The configuration interaction,[12–16] a numerically exact treatment, serves as the benchmark for usually adopted approximations. The simplest one is the Heitler-London ansatz in which one particle in the orbital ground state per dot is considered. The exchange asymptotic in this model differs from the exact[17,18] and the method fails completely in finite magnetic fields. Extensions of the single-particle basis include the Hund-Mullikan,[11] molecular orbital,[13,19] or variational method.[14,20] Other approaches, such as the Hartree-Fock,[21–23] random-phase approximation,[24] and (spin-)density functional theory[25] were also examined. None of them, however, is reliable in all important regimes,[4,15,26] which include weak/strong interdot couplings, zero/finite magnetic field, and symmetric/biased dot.

The spin-orbit interaction, a nonmagnetic spintronics workhorse,[27] is a generic feature in semiconductor quantum dots.[28] Although it is usually weak, it may turn out of major importance as, for example, for the spin relaxation[16,29–39] or, more positively, a handle for the electrical spin manipulation.[40–42] It is natural to expect that the presence of the spin-orbit interaction will influence the exchange Hamiltonian.[43] The resulting corrections to the rotationally symmetric exchange Hamiltonian are referred to as the anisotropic exchange (we do not consider other sources than the spin-orbit interaction[33,44–46]). Stringent requirements of the quantum computation algorithms motivate studies of the consequences of the anisotropic exchange of a general form on quantum gates.[47–49] Usually, the anisotropic exchange is viewed as a nuisance to be minimized.[50–52] On the other hand, it was considered as a possible way of implementing the quantum gates.[50,53] In both views, it is of utter importance to know the strength and the form of the anisotropic exchange. Since the spin-orbit interaction is weak, it is enough to answer the following question: what is the anisotropic exchange in the leading order?

Surprisingly, arriving at the answer was not straightforward at all. The Dzyaloshinskii-Moriya[54,55] interaction is of the first order in spin-orbit coupling. However, since it couples only states split by the isotropic exchange, it is necessary to consider also the second-order anisotropic exchange terms to arrive at correct energies.[56–58] Reference 59 suggested such a Hamiltonian, which was unitarily equivalent to the isotropic exchange Hamiltonian, with the exchange energy renormalized in the second order. This was later revisited,[60,61] with the following conclusion: in zero magnetic field, the two-qubit Hamiltonian is, up to the second order in the linear-in-momenta spin-orbit interaction, unitarily equivalent to the isotropic exchange Hamiltonian in the weak-coupling limit, with the unchanged exchange energy. Further corrections appear in the third order. In the unitary operator providing the change in the basis, the spin-orbit interaction appears in the linear order. These results are a consequence of the special form of the spin-orbit interaction, which in the leading order leads to a spatially dependent spin rotation.[62]

In the short version of this paper,[63] we derived the leading-order anisotropic exchange terms which appear in a

finite magnetic field. We derived all anisotropic exchange parameters in a form valid for arbitrary interdot coupling. We also compared the results obtained using the first-order versus the second-order treatment of the spin-orbit interactions. The main goal of the present work is a detailed assessment of the quantitative reliability of the presented anisotropic exchange model comparing with exact numerical results. Specifically, we examine the model in the strong- and weak-coupling regimes [corresponding to single (Sec. III) and double (Sec. IV) dots, respectively] and in zero and finite perpendicular magnetic field. We also study the role of the cubic Dresselhaus term (Sec. IV D), whose action does not correspond to a spatial texture (in the leading order) and could potentially become dominant over the linear terms, changing the picture considerably. In addition to that, we supply the derivations, not presented in the short version (Sec. II C) and a detailed account of our numerical method (Appendix A).

The analytical pitfalls in evaluating the isotropic exchange are well known.[17,64] On top of that, the anisotropic exchange is a (very) small correction to the exponentially sensitive isotropic exchange, and therefore it is involved to extract even numerically. Our main conclusion here is that the presented analytical model is valid in all studied regimes. Quantitatively, the effective parameters are usually within a factor of 2 from their counterparts derived from the numerically exact spectra. The main source of the discrepancy is the cubic Dresselhaus term. Surprisingly, in the most important regime for quantum dot spin qubits, namely, the weak coupling, the Heitler-London approximation works great for the anisotropic exchange, even though it fails badly for the isotropic one. This finding justifies using simple analytical formulas for the anisotropic exchange parameters.

II. MODEL

Our system is a two-dimensional electron gas confined in a [001] plane of a zinc-blende semiconductor heterostructure. An additional lateral potential with parabolic shape defines the double quantum dot. We work in the single band effective-mass approximation. The two-electron Hamiltonian is a sum of the orbital part and the spin-dependent part,

$$H_{tot} = H_{orb} + \sum_{i=1,2} H_{so,i} + H_{Z,i} = H_{orb} + H_{so} + H_Z, \qquad (1)$$

where the subscript i labels the two electrons. The orbital Hamiltonian is

$$H_{orb} = \sum_{i=1,2} (T_i + V_i) + H_C. \qquad (2)$$

Here, $T_i = \hbar^2 \mathbf{K}_i^2 / 2m$ is the kinetic energy with the effective mass m and the kinetic momentum $\hbar\mathbf{K}_i = \hbar\mathbf{k}_i + e\mathbf{A}_i = -i\hbar\boldsymbol{\nabla}_i + e\mathbf{A}_i$; e is the proton charge and $\mathbf{A}_i = B_z/2(-y_i, x_i)$ is the vector potential of the magnetic field $\mathbf{B} = (B_x, B_y, B_z)$. The potential V describes the quantum dot geometry

$$V_i = \frac{1}{2} m\omega_0^2 \min\{(\mathbf{r}_i - \mathbf{d})^2, (\mathbf{r}_i + \mathbf{d})^2\}. \qquad (3)$$

Here $l_0 = (\hbar/m\omega_0)^{1/2}$ is the confinement length, $2d$ measures the distance between the two potential minima, the vector $\mathbf{d}$ defines the main dot axis with respect to the crystallographic axes, and $E_0 = \hbar\omega_0$ is the confinement energy. The Coulomb interaction between the two electrons is

$$H_C = \frac{e^2}{4\pi\epsilon_0\epsilon_r} \frac{1}{|\mathbf{r}_1 - \mathbf{r}_2|}, \qquad (4)$$

where ϵ_0 is the vacuum dielectric constant and ϵ_r is the dielectric constant of the material.

The lack of the spatial inversion symmetry is accompanied by the spin-orbit interaction of a general form

$$H_{so,i} = \mathbf{w}_i \cdot \boldsymbol{\sigma}_i, \qquad (5)$$

where the vector $\mathbf{w}$ is kinetic momentum dependent. In the semiconductor heterostructure, there are two types of spin-orbit interactions. The Dresselhaus spin-orbit interaction, due to the bulk inversion asymmetry of the zinc-blende structure, consists of two terms, one linear and one cubic in momentum[28]

$$\mathbf{w}_{D,i} = \gamma_c \langle K_{z,i}^2 \rangle (-K_{x,i}, K_{y,i}, 0), \qquad (6)$$

$$\mathbf{w}_{D3,i} = \gamma_c/2 (K_{x,i} K_{y,i}^2, -K_{y,i} K_{x,i}^2, 0) + \text{H.c.}, \qquad (7)$$

here H.c. denotes the Hermitian conjugate. The interaction strength γ_c is a material parameter and the angular brackets in $\mathbf{w}_D$ denote the quantum averaging in the $\mathbf{z}$ direction. Since both electrons are in the ground state of the perpendicular confinement, we have $\langle K_{z,1}^2 \rangle = \langle K_{z,2}^2 \rangle = \langle K_z^2 \rangle$, the value depending on the confinement details. A confinement asymmetry along the growth direction (here $\mathbf{z}$) gives rise to the Bychkov-Rashba term[28]

$$\mathbf{w}_{BR,i} = \alpha_{BR} (K_{y,i}, -K_{x,i}, 0). \qquad (8)$$

The coupling α_{BR} of the interaction is structure dependent and can be, to some extent, experimentally modulated by the top gates potential. Equations (6)–(8) are valid for a coordinate system where the x and y axes are chosen along [100] and [010] directions, respectively. Below we use the effective spin-orbit lengths defined as $l_{br} = \hbar^2/2m\alpha_{BR}$ and $l_d = \hbar^2/2m\gamma_c\langle K_z^2 \rangle$.

The spin is coupled to the magnetic field through the Zeeman interaction

$$H_{Z,i} = \frac{g}{2} \mu_B \mathbf{B} \cdot \boldsymbol{\sigma}_i = \mu \mathbf{B} \cdot \boldsymbol{\sigma}_i, \qquad (9)$$

where g is the effective gyromagnetic factor, $\mu_B = e\hbar/2m_e$ is the Bohr magneton (alternatively, we use a renormalized magnetic moment μ) and $\boldsymbol{\sigma}$ is the vector of the Pauli matrices.

In lateral quantum dots the Coulomb energy E_C is comparable to the confinement energy and the correlation between the electrons strongly influence the states.[65,66] One can compare the energies considering

$$\frac{E_C}{E_0} = \frac{e^2}{4\pi\epsilon_0\epsilon_r}\langle r^{-1}\rangle \frac{ml_0^2}{\hbar^2} \sim \frac{l_0^2}{l_C\langle r\rangle}, \tag{10}$$

where the Coulomb length $l_C = e^2 m/4\pi\epsilon_0\epsilon_r\hbar^2$ is a material parameter and $\langle r\rangle$ is the mean distance between the electrons. In GaAs $l_C \approx 10$ nm, while a typical lateral dot has $l_0 \approx 30$ nm, corresponding to $E_0 \approx 1$ meV. The mean length $\langle r\rangle$ is on the order of the confinement length, if the two electrons are on the same dot, and of the interdot distance, if the electrons are on different dots. In the first case, the Coulomb energy is typically 3 meV. In the second case (one electron per dot) the Coulomb interaction is typically at least 1 meV.

The strength of the Coulomb interaction precludes the use of perturbative methods. Therefore, to diagonalize the two-electron Hamiltonian Eq. (1), we use the exact numerical treatment, the configuration interaction method. Details are given in Appendix A. Below we consistently use the notation of Φ for spinor and Ψ for orbital wave functions. They fulfill the equations $H_{tot}\Phi = E\Phi$ and $H_{orb}\Psi = E\Psi$, respectively.

We use the GaAs realistic parameters: $m = 0.067 m_e$ (m_e is the free-electron mass), $g = -0.44$, $\epsilon_r = 12.9$, and $\gamma_c = 27.5$ eV Å^3. The coupling of the linear Dresselhaus term is $\gamma_c\langle K_z^2\rangle = 4.5$ meV Å and of the Bychkov-Rashba term is $\alpha_{BR} = 3.3$ meV Å, corresponding to the effective spin-orbit lengths $l_d = 1.26$ μm and $l_{br} = 1.72$ μm, according to the recent experiments.[29,67] We use the confinement energy $\hbar\omega_0 = 1.1$ meV, which corresponds to the confining length $l_0 = 32$ nm, in line with an experiment.[68]

A. Unitarily transformed Hamiltonian

Analytically, we will analyze the role of the spin-orbit interactions in the two-electron spectrum using the perturbation theory. This approach is appropriate since the spin-orbit energy corrections are small compared to the typical confinement energy. For a GaAs quantum dot the ratio between the confinement length and the spin-orbit length $l_0/l_{so} \sim 10^{-2}$–10^{-3}. Furthermore, for a magnetic field of 1 T, the ratio between the Zeeman energy and the confinement energy is $\mu B/E_0 \sim 10^{-2}$. Therefore the spin-orbit interactions are small perturbations, comparable in strength to the Zeeman term at $B = 1$ T.

We consider the perturbative solution of Hamiltonian (1). We transform the Hamiltonian to gauge out the linear spin-orbit terms[62,69] (we neglect the cubic Dresselhaus term in the analytical models),

$$H_{tot} \to UH_{tot}U^\dagger = H_{orb} + H_Z + \bar{H}_{so}, \tag{11}$$

using the operator

$$U = \exp\left(-\frac{i}{2}\mathbf{n}_1\cdot\boldsymbol{\sigma}_1 - \frac{i}{2}\mathbf{n}_2\cdot\boldsymbol{\sigma}_2\right), \tag{12}$$

where

$$\mathbf{n}_i = \left(\frac{x_i}{l_d} - \frac{y_i}{l_{br}}, \frac{x_i}{l_{br}} - \frac{y_i}{l_d}, 0\right). \tag{13}$$

Keeping only terms up to the second order in the spin-orbit and Zeeman couplings, we get the following effective spin-orbit interactions $\bar{H}_{so} = H_{so}^{(2)} + H_Z^{(2)}$, where

$$H_{so}^{(2)} = \sum_{i=1,2} (-K_+ + K_- L_{z,i}\sigma_{z,i}/\hbar), \tag{14}$$

$$H_Z^{(2)} = \sum_{i=1,2} -(\mu\mathbf{B}\times\mathbf{n}_i)\cdot\boldsymbol{\sigma}_i. \tag{15}$$

Here, $L_{z,i}/\hbar = x_i K_{y,i} - y_i K_{x,i}$ and

$$K_\pm = \left(\frac{\hbar^2}{4ml_d^2} \pm \frac{\hbar^2}{4ml_{br}^2}\right). \tag{16}$$

Equation (15) describes the mixing between the Zeeman and spin-orbit interactions, which is linear in the spin-orbit couplings. It disappears in zero magnetic field, where only the terms in Eq. (14) survive—a sum of an overall constant shift of $2K_+$ and the spin-angular momentum operators. Both of these are quadratic in the spin-orbit couplings.

The point of the transformation, which changes the form of the spin-orbit interactions, is that the transformed interactions are much weaker (being the second, instead of the first order in the spin-orbit/Zeeman couplings). Of course, both Hamiltonians are equivalent, giving the same exact energies. However, a perturbative expansion of the transformed Hamiltonian converges much faster.

B. Orbital functions symmetry

The symmetry of the two-electron wave functions Ψ has important consequences, for example, in the form of selection rules for the couplings between the states due to the spin-orbit interactions. The choice of the potential in Eq. (3) is motivated by the fact that for small ($d \to 0$) and large ($d \to \infty$) interdot distance the eigenstates of the single-particle Hamiltonian converge to the single-dot solutions centered at $d = 0$ and $x = \pm 2d$, respectively. For zero magnetic field, since the double-dot potential does not have the rotational symmetry around the z axis, the inversions of the coordinate along axes of the confinement potential (x and y) are the symmetries involved. Indeed, the orbital Hamiltonian (2) commutes with the inversion operator I_x and I_y, $[H_{orb}, I_{x,y}] = 0$. Furthermore $[H_{orb}, I] = 0$, where $I = I_x I_y$ is the inversion of both axes simultaneously. All these operations belong to the C_{2v} group. Accordingly, the wave functions transform as the functions 1, x, xy, and y, which represent this group. If a perpendicular magnetic field is applied, only the total inversion operation, $I = I_x I_y$, commutes with the Hamiltonian and the wave function is symmetric or antisymmetric with respect to the total inversion—this is due to the lack of I_x and I_y symmetries of the kinetic-energy operator. The Slater determinants (the two-electron basis that we use in the diagonalization procedure—see Appendix A) have also definite symmetries, if they are built from single-particle states of definite symmetry (see Appendix B).

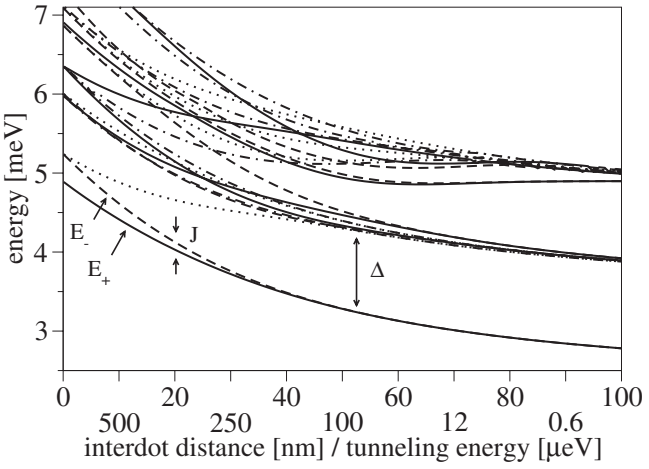

FIG. 1. Two-electron energy spectrum of a double dot at zero magnetic field as a function of the interdot distance and the tunneling energy. The spatial symmetries of wave functions, 1, x, xy, and y are denoted as solid, dashed, dotted-dashed, and dotted line, respectively. The two lowest energies are labeled; they are split by the isotropic exchange energy J. The energy separation between the lowest states and the higher exited states is denoted by Δ.

We define the functions $\Psi_\pm$ to be the lowest eigenstates of the orbital part of the Hamiltonian, $H_{orb}\Psi_\pm = E_\pm \Psi_\pm$ with the following symmetry:

$$P\Psi_\pm = \pm \Psi_\pm, \tag{17}$$

where $Pf_1g_2 = f_2g_1$ is the particle exchange operator. We observe that $\Psi_\pm$ have, in addition to the particle exchange symmetry, also a definite spatial symmetry. In further we assume they fulfill

$$I_1 I_2 \Psi_\pm = \pm \Psi_\pm. \tag{18}$$

We point out that while Eq. (17) is a definition, Eq. (18) is an assumption based on an observation. In zero magnetic field $I_1I_2\Psi_+ = +\Psi_+$, follows from the Mattis-Lieb theorem.[1] For the validity of Eq. (18) we resort to numerics—we saw it to hold in all cases we studied.

Figure 1 shows the calculated double-dot spectrum at zero magnetic field without the spin-orbit interactions. The two lowest states $\Psi_\pm$ are split by the exchange energy J. In the single-dot case ($d=0$), the ground state is nondegenerate while the first excited state is doubly degenerate. Increasing the interdot distance, this degeneracy is removed, as the two states have different spatial symmetries (x and y). The energy of the states $\Psi_\pm$ is separated from the higher states by an energy gap Δ. This gap allows us to consider only the two lowest orbital states when studying the spin-orbit influence on the lowest part of the two-electron spectrum. Indeed, in the double dot Δ is on the order of 1 meV while the spin-orbit interactions are two orders of magnitude smaller. In the case of $\Delta=0$, the two orbital states approximation can be improved including more states (although we show below this is not in fact necessary for a qubit pair in a circular dot).

Without the spin-orbit interactions, the eigenstates of Hamiltonian (1) are separable in the spin and orbital degrees of freedom. We get the four lowest states by supplementing $\Psi_\pm$ with spinors, forming the singlet and triplets,

$$\{\Phi_i\}_{i=1,\ldots,4} = \{\Psi_+ S, \Psi_- T_0, \Psi_- T_+, \Psi_- T_-\}. \tag{19}$$

Here $S = 1/\sqrt{2}(|\uparrow\downarrow\rangle - |\downarrow\uparrow\rangle)$ is a singlet spinor built out of two spin-1/2 spinors, $T_0 = 1/\sqrt{2}(|\uparrow\downarrow\rangle + |\downarrow\uparrow\rangle)$, $T_+ = |\uparrow\uparrow\rangle$, and $T_- = |\downarrow\downarrow\rangle$ are the three possible triplets; the quantization axis is chosen along the magnetic field.

The symmetry leads to selection rules for the matrix elements between two-electron states. In zero perpendicular magnetic field, because the L_z operator transforms as xy, the singlet and triplets are not coupled, up to the second order in the spin-orbit interactions, $\langle\Phi_1|\bar{H}_{so}|\Phi_{2,3,4}\rangle = 0$. The only contribution is due to the constant K_+. For nonzero perpendicular magnetic field, the singlet and a triplet are coupled only if their orbital parts have the opposite spatial symmetry due to the term in Eq. (15). The nonvanishing matrix elements are listed in Table I.

TABLE I. Conditions on the orbital symmetries for the matrix elements $\langle\Psi_1|\hat{O}|\Psi_2\rangle$ to be nonzero. The orbital symmetries are defined by $I\Psi_{1,2} = j_{1,2}\Psi_{1,2}$.

$\hat{O}$	Zero perpendicular field	Finite perpendicular field
$L_{z,1}$	Never	$j_1 = j_2$
$\mathbf{n}_1$	$j_1 \neq j_2$	$j_1 \neq j_2$

C. Effective Hamiltonians

Here we derive effective four level Hamiltonians, which provide understanding for the numerical results. We follow two different approaches: (i) restriction of the total Hamiltonian, Eq. (1), to the basis in Eq. (19) and (ii) including higher excited states through a sum rule using the Schrieffer-Wolff transformation with the unitary operator, Eq. (12). Then we compare the two models, including their simplifications using the Heitler-London approximation, to demonstrate the quality of their description of the two-qubit subspace.

We restrict the Hilbert space of the double dot to the four lowest functions Eq. (19) to describe the qubit pair. We start with the case of zero spin-orbit interactions. In the external magnetic field, the two triplets T_+ and T_- are split by twice the Zeeman energy $E_Z = 2\mu B_z$. The restriction of Hamiltonian (1) to the basis Eq. (19) produces a diagonal matrix

$$H_{iso} = \mathrm{diag}(E_+, E_-, E_- + E_Z, E_- - E_Z). \tag{20}$$

The standard notation is to refer only to the spinor part of the basis states. The matrix Eq. (20) can be rewritten in a more compact way using the basis of the 16 sigma matrices, $\{\sigma_{\alpha,1}\sigma_{\beta,2}\}_{\alpha,\beta=0,x,y,z}$ (index 0 denotes a unit matrix; for explicit expressions see Appendix D). The result is the so-called isotropic exchange Hamiltonian (where the constant $E_- - J/4$ was subtracted)

$$H_{iso} = (J/4)\boldsymbol{\sigma}_1 \cdot \boldsymbol{\sigma}_2 + \mu\mathbf{B}\cdot(\boldsymbol{\sigma}_1 + \boldsymbol{\sigma}_2), \tag{21}$$

where the singlet and triplets are separated by the isotropic exchange energy $J = E_- - E_+$, the only parameter of the model.

Hamiltonian (21) describes the coupling of the spins in the Heisenberg form. With this form, the SWAP gate can be performed as the time evolution of the system, assuming the exchange coupling J is controllable. The isotropic exchange has already been studied analytically, in the Heitler-London, Hund-Mulliken, Hubbard, variational and other approximations, as well as numerically using the finite-difference method. Usually analytical methods provide a result valid within certain regime of the external parameters only and a numerical calculation is needed to assess the quality of various analytical models.

When the spin-orbit interactions are included, additional terms in the effective Hamiltonian appear, as the matrix elements due to the spin-orbit interactions $(H'_{aniso})_{ij} = \langle \Phi_i | H_{so} | \Phi_j \rangle$. Selection rules in Table I restrict the nonzero matrix elements to those between a singlet and a triplet,

$$H'_{aniso} = \begin{pmatrix} 0 & 2\bar{w}_z & -\sqrt{2}u & \sqrt{2}v \\ 2\bar{w}_z^* & 0 & 0 & 0 \\ -\sqrt{2}u^* & 0 & 0 & 0 \\ \sqrt{2}v^* & 0 & 0 & 0 \end{pmatrix}. \tag{22}$$

Here $u=(\bar{w}_x+i\bar{w}_y), v=(\bar{w}_x-i\bar{w}_y)$ and

$$\bar{\mathbf{w}} = \langle \Psi_+ | \mathbf{w}_1 | \Psi_- \rangle, \tag{23}$$

where vector $\mathbf{w}$ is defined by the spin-orbit interactions Eq. (5). Using the sigma matrix notation, Eq. (22) can be written as (see Appendix D)

$$H'_{aniso} = \mathbf{a}' \cdot (\boldsymbol{\sigma}_1 - \boldsymbol{\sigma}_2) + \mathbf{b}' \cdot (\boldsymbol{\sigma}_1 \times \boldsymbol{\sigma}_2), \tag{24}$$

where the $\mathbf{a}'$ and $\mathbf{b}'$ are the spin-orbit vectors defined as

$$\mathbf{a}' = \mathrm{Re}\langle \Psi_+ | \mathbf{w}_1 | \Psi_- \rangle, \tag{25a}$$

$$\mathbf{b}' = \mathrm{Im}\langle \Psi_+ | \mathbf{w}_1 | \Psi_- \rangle. \tag{25b}$$

The standard exchange Hamiltonian follows as

$$H'_{ex} = H_{iso} + H'_{aniso} \tag{26}$$

and we refer to it in further as the first order (effective model) to point the order in which the spin-orbit interactions appear in the matrix elements. Note that we repeated the derivation of Ref. 59 additionally including the external magnetic field. As we will see below, comparison with numerics shows that treating the spin-orbit interactions to the linear order only is insufficient.

To remedy, we generalize the procedure of Ref. 60 to finite magnetic fields. This amounts to repeating the derivation that lead to Eq. (20), this time starting with the unitarily transformed Hamiltonian (11). In this way, the linear spin-orbit terms are gauged out and the resulting effective Hamiltonian treats the spin-orbit interactions in the second order in small quantities (the spin-orbit and the Zeeman couplings). The transformation asserts that the original Schrödinger equation $H_{tot}\Phi = E\Phi$ can be equivalently solved in terms of the transformed quantities $\bar{H}_{tot}(U\Phi) = E(U\Phi)$, with the Hamiltonian $\bar{H} = UH_{tot}U^\dagger$. The transformed Hamiltonian $\bar{H}$ is the same as the original, Eq. (1), except for the linear spin-orbit interactions, appearing in an effective form $\bar{H}_{so}$. We again restrict the basis to the lowest four states and for the spin-orbit contributions we get

$$(H_{aniso})_{ij} = \langle \Phi_i | \bar{H}_{so} | \Phi_j \rangle. \tag{27}$$

Using the selection rules and the algebra of the Pauli matrices, we get the exchange Hamiltonian (for obvious reasons, we refer to it as the second-order model)

$$H_{ex} = (J/4)\boldsymbol{\sigma}_1 \cdot \boldsymbol{\sigma}_2 + \mu(\mathbf{B} + \mathbf{B}_{so}) \cdot (\boldsymbol{\sigma}_1 + \boldsymbol{\sigma}_2) + \mathbf{a} \cdot (\boldsymbol{\sigma}_1 - \boldsymbol{\sigma}_2) + \mathbf{b} \cdot (\boldsymbol{\sigma}_1 \times \boldsymbol{\sigma}_2) - 2K_+. \tag{28}$$

Compared to the first-order model Eq. (24), the functional form of the second-order model Hamiltonian is the same, except for the effective spin-orbit magnetic field

$$\mu \mathbf{B}_{so} = \hat{\mathbf{z}}(K_-/\hbar)\langle \Psi_- | L_{z,1} | \Psi_- \rangle, \tag{29}$$

which appears due to an inversion symmetric part of $\bar{H}_{so}$, Eq. (14). The spin-orbit vectors, however, are qualitatively different

$$\mathbf{a} = \mu \mathbf{B} \times \mathrm{Re}\langle \Psi_+ | \mathbf{n}_1 | \Psi_- \rangle, \tag{30a}$$

$$\mathbf{b} = \mu \mathbf{B} \times \mathrm{Im}\langle \Psi_+ | \mathbf{n}_1 | \Psi_- \rangle. \tag{30b}$$

We remind that the second-order effective model Hamiltonian (28) refers to the four functions in Eq. (19) unitarily transformed $\{U\Phi_i\}_{i=1,\ldots,4}$. The agreement between the second-order effective model and the numerical data is very good, as we will see below.

D. First-order effective Hamiltonian in zero field

In this section we give H'_{ex} explicitly for zero B and diagonalize it. This is the only case for which is possible to give an analytical solution. For zero magnetic field, one can choose the functions $\Psi_\pm$ to be real. Then the matrix elements of the spin-orbit operator $\mathbf{w}$ in Eq. (5) are purely imaginary and $\mathbf{a}' = \mathbf{0}$. With the spin-quantization axis chosen along the vector $\mathbf{b}'$, the 4×4 matrix, Eq. (26), takes the form of

$$H'_{ex} = \begin{pmatrix} -3J/4 & 2ib' & 0 & 0 \\ -2ib' & J/4 & 0 & 0 \\ 0 & 0 & J/4 & 0 \\ 0 & 0 & 0 & J/4 \end{pmatrix}. \tag{31}$$

The upper left 2×2 block of this matrix is a Hamiltonian of a spin 1/2 particle in a fictitious magnetic field $\mathcal{B} = (0, 2b', J/2)/\mu$. The eigenstates of this Hamiltonian are spins oriented along the magnetic field $\mathcal{B}$. Since the matrix in Eq. (31) is block diagonal, it is easy to see that it can be diagonalized with the help of the following matrix:

$$\Sigma = \begin{pmatrix} 0 & 1 & 0 & 0 \\ 1 & 0 & 0 & 0 \\ 0 & 0 & 0 & 0 \\ 0 & 0 & 0 & 0 \end{pmatrix}. \tag{32}$$

Hamiltonian (31) can be diagonalized by $H_{diag} = \Theta H'_{ex} \Theta^\dagger$,

$$H_{diag} = \begin{pmatrix} -J/4 - |\mu\mathcal{B}| & 0 & 0 & 0 \\ 0 & -J/4 + |\mu\mathcal{B}| & 0 & 0 \\ 0 & 0 & J/4 & 0 \\ 0 & 0 & 0 & J/4 \end{pmatrix}, \quad (33)$$

where $|\mu\mathcal{B}|^2 = 4(b')^2 + J^2/4$. In the notation of the Pauli matrices, (see Appendix D),

$$\Theta = \exp\left(-i\frac{\Sigma\theta}{2}\right) = \exp\left[-\frac{i}{4}\theta(\sigma_{\mathcal{B},1} - \sigma_{\mathcal{B},2})\right], \quad (34)$$

where $\tan\theta = 4b'/J$ and $\sigma_{\mathcal{B}} \equiv \boldsymbol{\sigma}\cdot\mathcal{B}/\mathcal{B}$.

The unitary transformation Θ in Eq. (34) performs the rotation of the two spins in the opposite sense. The Hamiltonian can be interpreted as a rotation of the electron around a spin-orbit field when transferred from one dot to the other.[59] The spectrum given by Eq. (33) qualitatively differs from the numerics, which shows there is no influence on the exchange in the second order of the spin-orbit couplings.

III. SINGLE DOT

We start with the single-dot case, corresponding in our model to $d=0$. The analytical solution of the single-particle Hamiltonian $T+V$ is known as the Fock-Darwin spectrum. The corresponding wave functions ψ and the energies ϵ are

$$\psi_{nl}(r_i, \varphi_i) = C\rho_i^{|l|} e^{-\rho_i^2/2} L_n^{|l|}(\rho_i^2) e^{il\varphi_i}, \quad (35)$$

$$\epsilon_{nl} = \frac{\hbar^2}{ml_B^2}(2n + |l| + 1) + B\frac{e\hbar}{2m}l, \quad (36)$$

where $\rho_i = r_i/l_B$ and $l_B = [l_0^{-4} + (eB_z/2\hbar)^2]^{-1/4}$ is the magnetic length; n and l are the radial and the angular quantum numbers, C is the normalization constant, and $L_n^{|l|}$ are the associated Laguerre polynomials.

Let us consider now the orbital two-electron states Ψ, eigenstates of H_{orb}, Eq. (2). The Coulomb operator H_C commutes with the rotation of both electrons around the z axis, that is, the Coulomb interaction couples only states with the same total angular momentum. This allows us to label the states with the quantum number $L = L_1 + L_2$, the total angular momentum. Furthermore, the Hamiltonian H_{orb} commutes with any spin rotation of any of the electrons, which expresses the fact that the Coulomb interaction conserves spin. Therefore we can consider the full two-electron wave functions obtained by supplementing the orbital part Ψ with a spinor, respecting the overall wave-function symmetry, similarly as in Eq. (19).

The two-electron spectrum, without the Zeeman and the spin-orbit interactions, is shown in Fig. 2. At zero magnetic field the ground state is a nondegenerate singlet state with total angular momentum zero $L=0$. The next two degenerate states are triplets with $L = \pm 1$ and their degeneracy is split by the magnetic field. Focusing on the two lowest states, most relevant for the qubit pair, they cross at $B \approx 0.43$ T, so one can turn the ground state from the singlet to the triplet by applying an external magnetic field. In the presence of spin-orbit interactions, the crossing is turned into anticrossing, as described below.

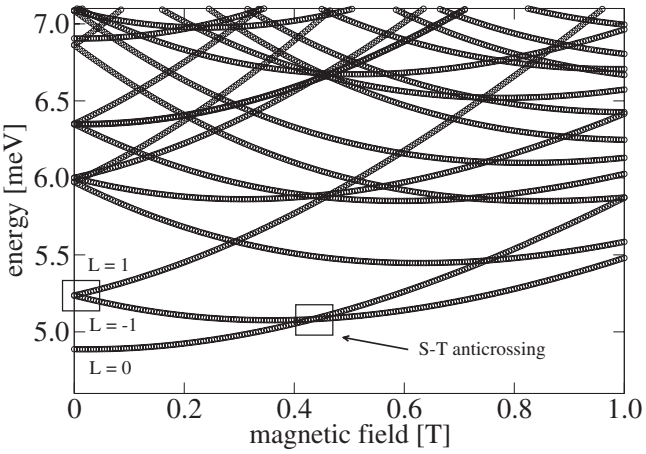

FIG. 2. Two-electron energy spectrum of a single dot in perpendicular magnetic field. The lowest states are labeled by the total angular momentum L. The Zeeman and spin-orbit interactions are neglected. The two regions marked by boxes are magnified in Figs. 3 and 4.

Spin-orbit correction to the energy spectrum in magnetic field

Suppose some parameter, such as the magnetic field, is being changed. It may happen at some point that the states of the opposite spin become degenerate. Such points are called spin hot spots. Here, because of the degeneracy, weak spin-orbit interactions have strong effects. For the spin relaxation, spin hot spots play often a dominant role.[70]

We are interested in the changes to the spectrum due to the spin-orbit interactions. Let us neglect the cubic Dresselhaus in this section. To understand the spin-orbit influence, it is important to note the following commutation relations for the linear spin-orbit terms:

$$[\mathbf{w}_{BR,1}\cdot\boldsymbol{\sigma}_1 + \mathbf{w}_{BR,2}\cdot\boldsymbol{\sigma}_2, \hat{J}_+] = 0,$$

$$[\mathbf{w}_{D,1}\cdot\boldsymbol{\sigma}_1 + \mathbf{w}_{D,2}\cdot\boldsymbol{\sigma}_2, \hat{J}_-] = 0, \quad (37)$$

where $\hat{J}_\pm = \Sigma_i(\hat{L}_{z,i} \pm \hat{S}_{z,i})$. These commutation rules hold for any magnetic field B. Since Hamiltonian (2) commutes with the operator $\hat{J}_\pm$, we can label the states using the quantum numbers $J_+ = L + S_z$ and $J_- = L - S_z$. The spin-orbit interactions couple only the states with the same quantum numbers J_+ and J_-, for Bychkov-Rashba and Dresselhaus term, respectively.

Let us focus on the part of the spectrum close to $B=0$ and on the states with $L = \pm 1$, Fig. 2. The degeneracy of the states is removed by the spin-orbit interactions, as shown in Fig. 3.

Let us now use Hamiltonian (11), to understand the influence of the spin-orbit interactions. The degeneracy of the states with angular momenta $L = \pm 1$ makes the description with the lowest two orbital states questionable. Therefore

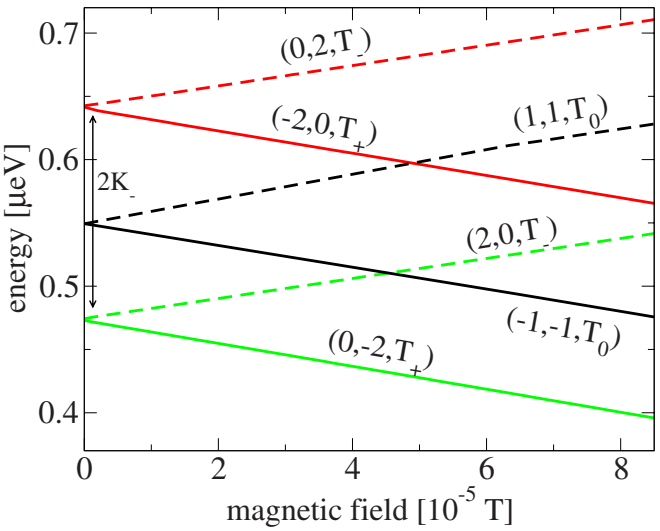

FIG. 3. (Color online) Magnified region from Fig. 2. Energy spectrum of a single dot for small perpendicular magnetic field. Only the states with the total angular momentum $L=\pm 1$ are plotted. A constant shift is removed from the spectrum. Each state is labeled by the quantum numbers (J_+, J_-, T_i).

now we take three orbital states and repeat the derivation of the second-order effective Hamiltonian, obtaining a 7×7 matrix. The basis functions are

$$\{\Phi_i\}_{i=1,\ldots,7} = \{\Psi_+ S, \Psi_- T_0, \Psi_- T_+, \Psi_- T_-, \Psi'_- T_0, \Psi'_- T_+, \Psi'_- T_-\}, \tag{38}$$

where Ψ_+ is the electron wave function with angular momentum $L=0$, and Ψ_- and Ψ'_- have angular momentum $L=+1$, and $L=-1$, respectively. Since the magnetic field is negligible with respect to the spin-orbit couplings, Hamiltonian (15) is negligible. Because of the selection rules, Table I, the contributions from Eq. (14) in the basis Eq. (38), gives nonzero matrix elements only for the following pairs, $\langle \Psi_- T_\pm | \bar{H}_{so} | \Psi_- T_\pm \rangle = \pm K_-$ and $\langle \Psi'_- T_\pm | \bar{H}_{so} | \Psi'_- T_\pm \rangle = \pm K_-$. For the GaAs parameters, $K_-=0.16$ μeV. In the region of small magnetic field, the states with $J_\pm=0$ are coupled by the spin-orbit interactions and the lifting is in the second order in the spin-orbit couplings. The other states are not coupled since they have different values of $J_\pm$. Therefore we conclude that the two-orbital state approximation can be used also for the single-dot case (or strongly coupled double dots) because the spin-orbit interactions do not mix the states Ψ and Ψ' in the basis Eq. (38). Note that as the coupling is forbidden by the inversion symmetry, the claim holds for an arbitrary oriented magnetic field.

Let us now discuss the second degeneracy region marked in Fig. 2, magnified in Fig. 4. The spin-orbit interactions induce two anticrossings. The first is due to the Bychkov-Rashba term, since the crossing states have different J_-, but the same $J_+=0$ and couples the singlet S and triplet T_+. The second is due to the Dresselhaus term which couples states with $J_-=0$, the singlet S and the triplet T_-. The central point is a crossing point because the crossing state differ in both J_+ and J_-. The splitting energy can be evaluated using the unitarily transformed Hamiltonian (11). Using the degenerate perturbation theory, one can estimate analytically, using Eqs. (14) and (15), the value of the two gaps to be $\Delta_{BR} \approx 4\sqrt{2}\mu B l_0 / l_{BR} = 0.15$ μeV and $\Delta_D \approx 4\sqrt{2}\mu B l_0 / l_D = 0.58$ μeV. These values are consistent with the numerical values.

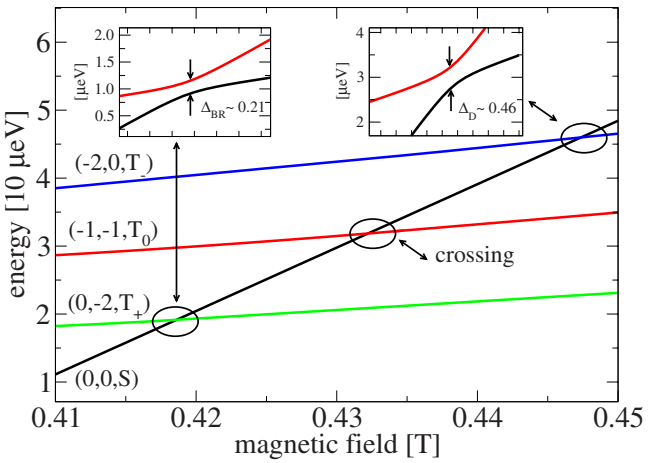

FIG. 4. (Color online) Lowest energy levels in the anticrossing region marked in Fig. 2. A constant shift was removed from the spectrum. The quantum numbers (J_+, J_-, Σ_i) label the states. Insets show the anticrossing regions.

IV. DOUBLE DOT

The double dot denotes the case when the interdot distance is on the order of the confinement length. In the next sections we discuss our effective models, Eqs. (26) and (28) in the double-dot regime and compare them with numerics.

A. Heitler-London approximation

The analytical solution for the two-electron wave functions in a double-dot potential is not known. We consider here the Heitler-London ansatz since it is a good approximation at large interdot distances and we can work out the spin-orbit influence on the spectrum analytically. For this purpose, we compute the spin-orbit vectors, Eqs. (24) and (29), for our models.

In the Heitler-London ansatz, the two-electron eigenfunctions are given by

$$\Psi_\pm = \frac{1}{\sqrt{2(1 \pm |\langle \psi_{L,1} | \psi_{R,1} \rangle|^2)}} (|\psi_{L,1}\rangle |\psi_{R,2}\rangle \pm |\psi_{R,1}\rangle |\psi_{L,2}\rangle), \tag{39}$$

where $|\psi_{L(R),i}\rangle$ is a single electron Fock-Darwin state centered in the left (right) dot occupied by the ith electron. Below, in Eqs. (39), (40a), (40b), (41a), (41b), and (42), we skip the particle subscript i, as the expressions contain only single-particle matrix elements (all ψ, w, n, and L_z would have the same subscript, say $i=1$). With this ansatz, the spin-orbit vectors, Eq. (24), follow as

$$\mathbf{a}' = \frac{1}{\sqrt{1-|\langle\psi_L|\psi_R\rangle|^4}}\langle\psi_L|\mathbf{w}|\psi_L\rangle, \tag{40a}$$

$$\mathbf{b}' = \frac{i}{\sqrt{1-|\langle\psi_L|\psi_R\rangle|^4}}\langle\psi_L|\mathbf{w}|\psi_R\rangle\langle\psi_R|\psi_L\rangle. \tag{40b}$$

Similarly we get the spin-orbit vectors, Eq. (29), as

$$\mathbf{a} = \frac{\mu}{\sqrt{1-|\langle\psi_L|\psi_R\rangle|^4}}\langle\psi_L|\mathbf{B}\times\mathbf{n}|\psi_L\rangle, \tag{41a}$$

$$\mathbf{b} = \frac{i\mu}{\sqrt{1-|\langle\psi_L|\psi_R\rangle|^4}}\langle\psi_L|\mathbf{B}\times\mathbf{n}|\psi_R\rangle\langle\psi_R|\psi_L\rangle, \tag{41b}$$

and the spin-orbit-induced magnetic field

$$\mu\mathbf{B}_{so} = \hat{\mathbf{z}}\frac{K_-/\hbar}{1-|\langle\psi_L|\psi_R\rangle|^2}(\langle\psi_L|L_z|\psi_L\rangle + -\langle\psi_L|L_z|\psi_R\rangle\langle\psi_R|\psi_L\rangle). \tag{42}$$

The explicit formulas for the vectors in Eqs. (39), (40a), (40b), (41a), (41b), and (42) are in Appendix C. Differently from the spin-orbit vectors in Eq. (39), the vectors in Eq. (40) reveal explicitly the anisotropy with respect to the magnetic field and dot orientation[71,72] [note that x and y in the definition of $\mathbf{n}$, Eq. (13) are the crystallographic coordinates].

B. Spin-orbit correction to the energy spectrum in zero magnetic field

In the previous sections, we have derived two effective Hamiltonians, H'_{ex}, and H_{ex}, given by Eqs. (28) and (29) and Eqs. (24), (25a), (25b), and (26), respectively. We now compare the energy spectrum given by these models with exact numerics. We present the spin-orbit-induced energy shift, the difference between a state energy if the spin-orbit interactions are considered and artificially set to zero. For each model we examine also its Heitler-London approximation, which yields analytical expressions for the spin-orbit vectors, as well as the isotropic exchange energy (given in Sec. IV A and Appendix C). Thus, the effective models in the Heitler-London approximation (we denote them by superscript HL) are fully analytic. The nonsimplified models (we refer to them as "numerical") require the two lowest exact double-dot two-electron wave functions, which we take as numerical eigenstates of H_{orb}.

Apart from the energies, we compare also the spin-orbit vectors. Since they are defined up to the relative phase of states Ψ_+ and Ψ_-, the observable quantity is $c' = \sqrt{(a')^2 + (b')^2}$ and analogously for $c = \sqrt{a^2+b^2}$. We refer to these quantities as the anisotropic part of the exchange coupling. Figure 5 shows the spin-orbit-induced energy shift as a function of the interdot distance for each of the four states.

The exact numerics gives a constant and equal shift for all four spin states, with value -0.54 μeV. Let us consider the second-order model, Eq. (28). For zero magnetic field, all spin-orbit vectors are zero, as is the effective magnetic field. The only contribution comes from the constant term $2K_+ = -0.54$ μeV that is the same for all states. Our derived spin model, Eq. (28), accurately predicts the spin-orbit contributions to the energy. On the other hand, the first-order models H'^{HL}_{ex} and H'_{ex} are completely off on the scale of the spin-orbit contributions. The exchange Hamiltonian H'_{ex} does not predict the realistic spin-orbit influence on the spectrum, even in the simple case when the magnetic field is zero.

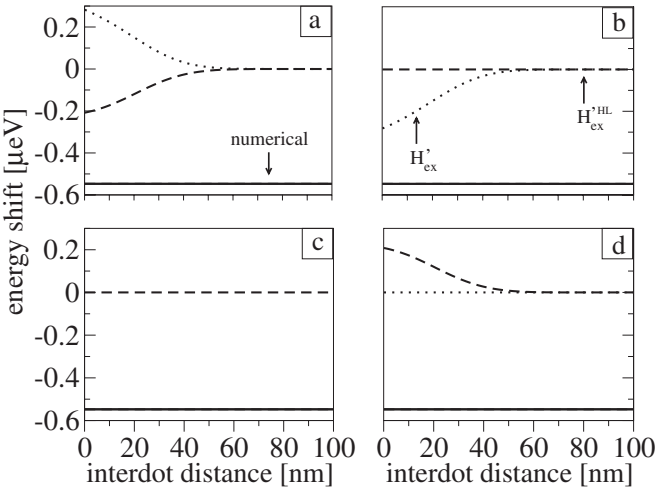

FIG. 5. Spin-orbit-induced energy shifts at zero magnetic field as a function of the interdot distance. Exact numerics (solid), first-order model H'_{ex} (dotted), and first-order model in HL approximation (dashed) are given. (a) Singlet, (b) triplet T_0, (c) triplet T_+, and (d) triplet T_-. The results of the second-order model (both H^{HL}_{ex} and H_{ex} give the same) are indiscernible from exact numerical data.

Figure 6 shows the nonzero parameters for all four models. The exact isotropic exchange J decays exponentially with the interdot distance. The same behavior is predicted in the Heitler-London approximation. It decays exponentially but deviates from the numerical results. As for the anisotropic exchange, the first-order model H'_{ex} gives an exponentially falling spin-orbit parameter c', an order of magnitude smaller than J. In contrast, the second-order model H_{ex} predicts zero spin-orbit anisotropic exchange. First main result, proved numerically and justified analytically by the Hamil-

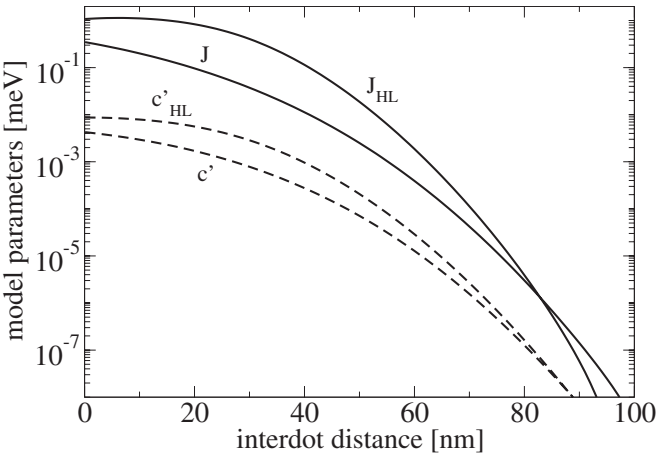

FIG. 6. Spin-orbit parameters at zero magnetic field as function of the interdot distance. Numerical value and the Heitler-London approximation for the isotropic exchange (solid) and the anisotropic exchange of the first-order model (dashed).

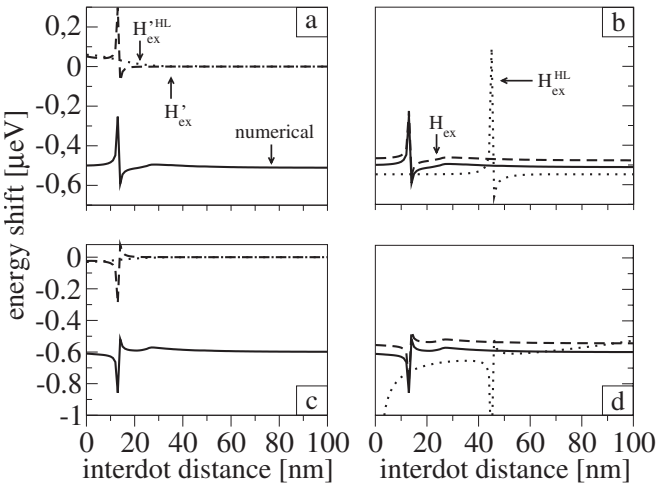

FIG. 7. Spin-orbit-induced energy shifts at 1 T perpendicular magnetic field versus the interdot distance. (a) Energy shift of the Singlet S in the exact numerics (solid) is compared to the numerical (dashed) and the Heitler-London approximation (dotted) first-order model. In (b) similar comparison is made for the second-order model. Panels (c) and (d) are analog of (a) and (b) showing the energy shifts of the triplet T_+.

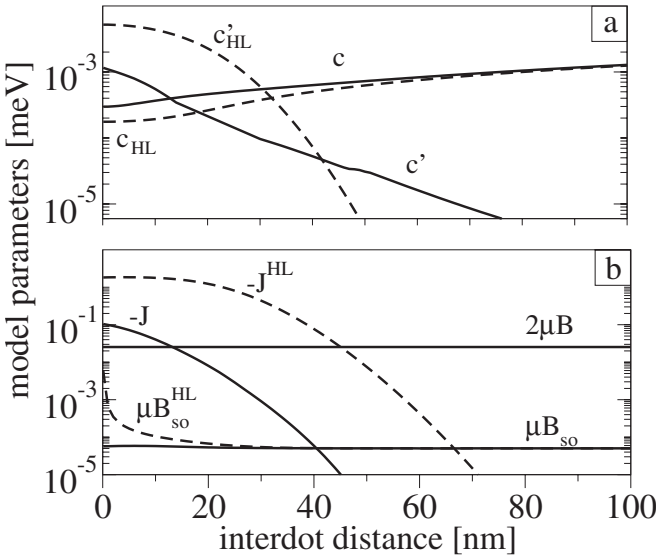

FIG. 8. Spin-orbit parameters at 1 T perpendicular magnetic field versus the interdot distance. (a) Numerical (solid) and Heitler-London approximation (dashed) anisotropic exchange vectors for the first- and second-order models. (b) Isotropic exchange, Zeeman energy, and the spin-orbit-induced effective magnetic field.

tonian H_{ex}, is that *at zero magnetic field the spin-orbit vectors vanish*, up to the second order in spin-orbit couplings at any interdot distance. In the transformed basis, there is no anisotropic exchange at the zero magnetic field due the spin-orbit interactions, an important result for the quantum computation. Indeed, since the exchange energy can be used to perform a SWAP operation, this means that the spin-orbit interactions do not induce any significant errors on the gate operation. The only difference is the computational basis, which is unitarily transformed with respect to the usual singlet-triplet basis.

C. Finite magnetic field

In the presence of a perpendicular magnetic field the structure of the spin-orbit contributions are quite different with respect to the zero-field case. First of all, anticrossing points appear, where the energy shift is enhanced. Figure 7 shows the spin-orbit contributions in a finite magnetic field. We plot only the anticrossing states, the singlet S and the triplet T_+. The prediction of the first-order model is shown in the left panels of Fig. 7. As in the case of zero magnetic field, this model is off from the numerical results. In particular, it still predicts a zero contribution, except close to the anticrossing point. We note that the discrepancy is not connected to (a failure of) the Heitler-London approximation, as using the exact numerical two-electron wave functions does not improve the model predictions.

In the right panels of Fig. 7, the comparison between the second-order model and the numerics is provided. We observe that the model is very close to the numerics, even though the Heitler-London approximation predicts the crossing point in a different position. The predictions of the numerical second-order model H_{ex} are consistent with the exact numerics. The only discrepancy is due to the influence of the cubic Dresselhaus term, as we will see in the next section.

To get more insight, in Fig. 8 we have plotted the parameters of the models. Figure 8(a) shows the anisotropic exchange strengths in the two models. The first-order model H'_{ex} predicts the anisotropic exchange decreasing with the interdot distance, similar to the isotropic exchange energy. For large interdot distance the anisotropic exchange c' disappears. This means there is no influence on the energy due to the spin-orbit interactions. On the other hand, for the second-order model H_{ex} the conclusion is different. For large interdot distances c^{HL} and c are linear in d. Furthermore, the anisotropic exchange computed in the Heitler-London ansatz is very close to the numerical one. We make a very important observation here: surprisingly, concerning the anisotropic exchange the Heitler-London is quite a good approximation for all interdot distances even in a finite magnetic field. Therefore, despite its known deficiencies to evaluate the isotropic exchange J, it grasps the anisotropic exchange even quantitatively, rendering the spin-orbit part of the second-order effective Hamiltonian H_{ex} fully analytically. One can understand this looking at Eq. (29). The anisotropic exchange vectors are given by the dipole moment of the matrix element between the left and right localized states (see Appendix C for explicit formula). This dipole moment is predominantly given by the two local maxima of the charge distribution (the two dots) and is not sensitive to the interdot barrier details, nor on the approximation used to estimate the lowest two orbital two-electron states. This is in strong contrast to the isotropic exchange, which, due to its exponential character, depends crucially on the interdot barrier and the used approximation.

Figure 8(b) shows the isotropic exchange J and the effective magnetic field induced by the spin-orbit interactions μB_{so} compared to the Zeeman energy $2\mu B$. We see the failure of the Heitler-London approximation for J. Although the

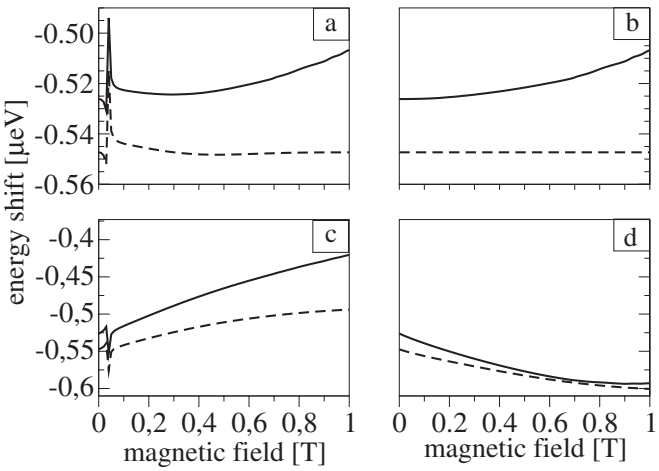

FIG. 9. Spin-orbit-induced energy shifts of a double-dot system with interdot distance of 55 nm versus the perpendicular magnetic field. (a) singlet S, (b) triplet T_0, (c) triplet T_+, and (d) triplet T_-. Exact numerics (solid) and the numerical second-order model H_{ex} (dashed).

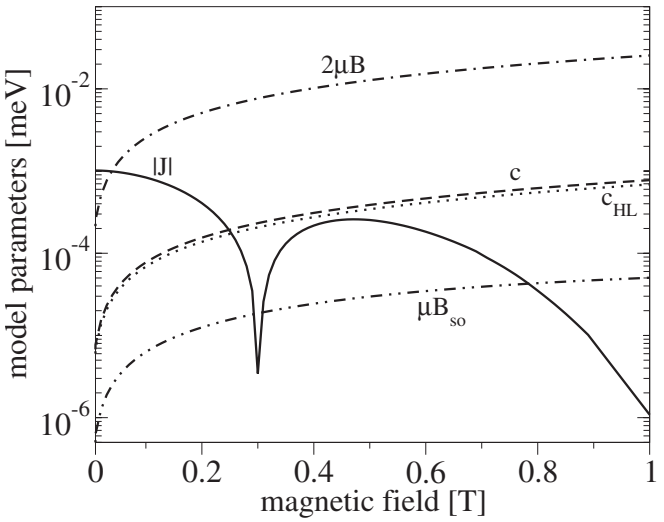

FIG. 10. Spin-orbit parameters of the second-order numerical model H_{ex} in a double-dot system with interdot distance of 55 nm versus the magnetic field.

numerical calculation and the analytical prediction have the same sign (this means that the ground state is the triplet) they differ by an order of magnitude. The Zeeman energy is constant and always much larger than the effective spin-orbit-induced magnetic field μB_{so}. Consequently, the effective field can be always neglected. The point where the Zeeman energy equals to the isotropic exchange (close to $d=18$ nm) is the anticrossing point, where the spin-orbit contributions are strongly enhanced, as one can see in Fig. 7.

Let us consider a double-dot system at fixed interdot distance of 55 nm, corresponding to zero-field isotropic exchange of 1 μeV. In Fig. 9 the spin-orbit contributions versus the magnetic field are plotted for the second-order model H_{ex} and the exact numerics. We can conclude that to describe the spin-orbit influence on the states in a double-dot system it is important to use the second-order Hamiltonian H_{ex}.

In Fig. 10 the spin-orbit parameters versus the magnetic field are plotted. The main influence on the spin is due to the Zeeman interaction in the whole range of B since μB_{so} is several orders of magnitude smaller than the Zeeman energy. At the ground-state anticrossing point, the isotropic exchange crosses zero while the anisotropic parameter c is finite, leading to spin hot spots. Apart from these, since the anisotropic exchange is two orders of magnitude smaller than the Zeeman energy, the spin-orbit-induced energy shifts are minute.

D. Cubic Dresselhaus contributions

Finally we consider the role of the cubic Dresselhaus term. The Schrieffer-Wolff transformation does not remove it in the linear order. Figure 11 shows the energy shifts induced by the spin-orbit interactions also in the case where we do not take into account the cubic Dresselhaus term. One can see a very good agreement between the second-order model H_{ex} and the exact numerics where the cubic Dresselhaus term was omitted. Therefore we can conclude that the main part of the discrepancy we see in the spin-orbit-induced energy shifts are due to the cubic Dresselhaus term.

V. CONCLUSIONS

We analyzed the spin-orbit influence on two electrons confined in a lateral double quantum dot. We focused on the lowest part of the Hilbert space, which corresponds to a qubit pair. In Ref. 63 the Hamiltonian for such pair was proposed, with the spin-orbit interactions giving rise to an anisotropic exchange interaction. Within a unitarily transformed basis, this interaction is encoded into two real three-dimensional spin-orbit vectors. These, together with the isotropic ex-

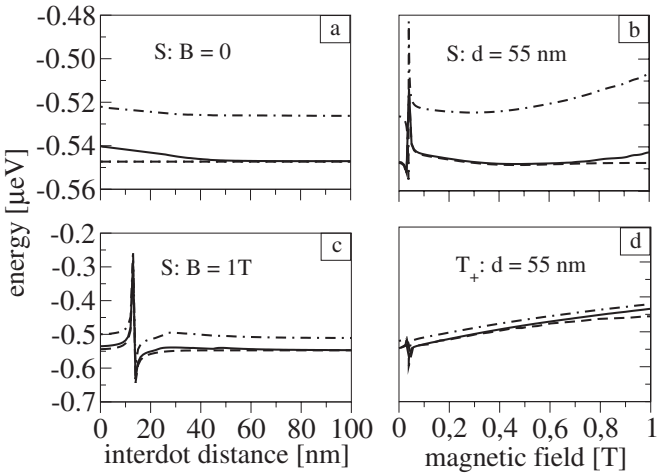

FIG. 11. The spin-orbit-induced energy shift as a function of the interdot distance (left panels) and perpendicular magnetic field (right panels). (a) Singlet in zero magnetic field, (c) singlet at 1 T field, (b) and (d) singlet and triplet T_+ at 55 nm. The numerical second-order model H_{ex} (dashed line), exact numerics (dot-dashed line), and exact numerics without the cubic Dresselhaus term (solid line).

change energy and the magnetic field vector, completely parametrize an effective two-qubit Hamiltonian. In this work, we examined the quantitative validity of this effective Hamiltonian.

In addition to a numerical study, we also provided the details of the effective Hamiltonian derivation, which were skipped in Ref. 63. We noted that it can be diagonalized analytically if the effective spin-orbit vectors are all aligned with the external magnetic field, the only exactly solvable case (apart from the trivial case of no spin-orbit interactions present). We also evaluated the spin-orbit vectors in the Heitler-London approximation and compared the analytical results with their exact numerical counterparts.

There are three possible sources for a discrepancy between the model and the exact data: the higher excited orbital states of the quantum dot, the higher orders of the effective (unitary transformed) spin-orbit interactions, and the cubic Dresselhaus term. Elucidation of their importance is one of the main results of this work. (i) We find the cubic Dresselhaus term is the main source of the discrepancy. In a typical double-dot regime and a moderate field of 1 T, it brings an error of ~ 0.1 μeV for the energies while the two other mentioned corrections have an order of magnitude smaller influence. (ii) We find the effective Hamiltonian describes both the weak- and the strong-coupling regimes (the single dot represents the strongest possible coupling). (iii) Surprisingly, the spin-orbit vectors obtained within the Heitler-London approximation are faithful even at a finite magnetic field. Overall, we find the anisotropic exchange Hamiltonian to be generally reliable, providing a realistic and yet simple description for an interacting pair of spin qubits realized by two-coupled quantum dots.

ACKNOWLEDGMENTS

We would like to thank Guido Burkard for useful discussion, Martin Gmitra and Andrea Nobile for numerical advice. This work was supported by DFG GRK 638, SPP 1285, SFB 689, NSF under Grant No. DMR-0706319, RPEU-0014-06, ERDF OP R&D Project "QUTE," CE SAS QUTE, and DAAD.

APPENDIX A: NUMERICAL METHOD

Here we describe the numerical method we use to diagonalize the two-electron Hamiltonian (1). We proceed in three steps.[73] We first diagonalize the single electron Hamiltonian $H=T+V$, using the numerical finite differences method with the Dirichlet boundary condition (vanishing of the wave function at boundaries). We do not consider the spin-dependent part (spin orbit, Zeeman) at this step. This allows us to exploit the symmetries of the confinement potential. The single electron Hamiltonian is diagonalized by the Lanczos method.[67] The typical number of points in the grid we use is 60×60, giving relative precision of the energy of order 10^{-6}.

In the second step, using the obtained single electron eigenstates $\{(\psi_i,\epsilon_i)\}$, we construct the two-electron states. We use them as a basis in which the two-electron orbital Hamiltonian (2) is diagonalized. The two-electron states are constructed as symmetric

$$|\Psi_s^{(i,j)}\rangle = \frac{1}{\sqrt{2}}(|\psi_{i,1}\rangle|\psi_{j,2}\rangle + |\psi_{j,1}\rangle|\psi_{i,2}\rangle) \quad \text{for} \quad i \neq j, \tag{A1}$$

$$|\Psi_s^{(i,j)}\rangle = |\psi_{i,1}\rangle|\psi_{j,2}\rangle \quad \text{for} \quad i = j, \tag{A2}$$

and antisymmetric

$$|\Psi_t^{(i,j)}\rangle = \frac{1}{\sqrt{2}}(|\psi_{i,1}\rangle|\psi_{j,2}\rangle - |\psi_{j,1}\rangle|\psi_{i,2}\rangle), \tag{A3}$$

with respect to the particle exchange. We choose $n_{s.e.}$ single electron orbitals, typically $n_{s.e.}=21$. The total number of the two-particle states is then $n_{s.e.}^2$.

The spatial symmetry allows us to reduce the dimension of the two-electron Hamiltonian matrix to diagonalize. Namely, the matrix is block diagonal, with the basis functions grouped according to the spatial symmetry $(1,x,y,xy)$ and particle exchange symmetry (± 1). This results in eight blocks and holds for zero perpendicular magnetic field. In a finite field, we get four blocks, as there are only two spatial symmetries possible (1 and x). Each block is diagonalized separately.

The matrix element of the two-electron Hamiltonian, Eq. (2), in our basis is

$$\langle \Psi_a^{(i,j)}|H_{orb}|\Psi_b^{(n,m)}\rangle = (\epsilon_i+\epsilon_j)\delta_{i,m}\delta_{j,n}\delta_{a,b} + \delta_{a,b}\int d\mathbf{r}_1 \int d\mathbf{r}_2 \Psi_a^{(i,j)} \times \frac{e^2}{4\pi\varepsilon_0\varepsilon_r}\frac{1}{|\mathbf{r}_1-\mathbf{r}_2|}\Psi_b^{(n,m)}. \tag{A4}$$

The last term in Eq. (A4) is due to the Coulomb interaction and it leads to off diagonal terms in the Hamiltonian. We diagonalize the matrix defined in Eq. (A4) to get the eigenspectrum $\{(\Psi_i,E_i)\}$.

In the third step, we add the spin-dependent parts to the Hamiltonian. We construct a new basis by expanding the wave functions obtained in the previous step by the spin. The orbital wave function Ψ_i gets the spinor according to its particle exchange symmetry. The symmetric function gets the singlet S while the antisymmetric appears in three copies, each with one of the three triplets T_0, T_+, and T_-. We denote the new states by

$$|\Phi_{i\Sigma}\rangle = |\Psi_i\rangle|\Sigma\rangle, \tag{A5}$$

where $|\Sigma\rangle$ corresponds to one of the four spin states. The matrix elements of the total Hamiltonian (1) are

$$\langle \Phi_{i\Sigma}|H_{tot}|\Phi_{i'\Sigma'}\rangle = E_i\delta_{i,i}\delta_{\Sigma,\Sigma'} + 2\mu|\mathbf{B}|(\delta_{\Sigma,T_+}-\delta_{\Sigma,T_-})\delta_{i,i}\delta_{\Sigma,\Sigma'} + \sum_{j=1,2}\langle\Psi_i|\mathbf{w}_j|\Psi_{i'}\rangle\cdot\langle\Sigma|\boldsymbol{\sigma}_j|\Sigma'\rangle, \tag{A6}$$

where the last term is the matrix element of the spin-orbit interactions. The resulting matrix is diagonalized to get the final eigenstates. We choose a certain number n_s of lowest Ψ_i

states, depending on the required precision. In our simulations $n_s=250$, resulting to the accuracy on the order of 10^{-5} meV for the energy.

Coulomb integral

Computationally most demanding are the Coulomb integrals. Indeed, the typical size of the Hamiltonian matrix, in the second step, is 441×441, requiring at least 10^6 Coulomb integrals. Writing functions involved in the Eq. (A4) as Slater determinants, we can express the integral as a sum of terms such as the following:

$$C_{ijkl}=\frac{e^2}{4\pi\varepsilon_0\varepsilon_r}\int d\mathbf{r}_1 d\mathbf{r}_2 \frac{\psi_i(\mathbf{r}_1)^*\psi_j(\mathbf{r}_2)^*\psi_k(\mathbf{r}_1)\psi_l(\mathbf{r}_2)}{|\mathbf{r}_1-\mathbf{r}_2|}$$

$$=\frac{e^2}{4\pi\varepsilon_0\varepsilon_r}\int d\mathbf{r}_1 d\mathbf{r}_2 \frac{\mathcal{F}_{ik}(\mathbf{r}_1)\mathcal{F}_{jl}(\mathbf{r}_2)}{|\mathbf{r}_1-\mathbf{r}_2|}, \tag{A7}$$

where $\mathcal{F}_{ik}(\mathbf{r})=\psi_i(\mathbf{r})^*\psi_k(\mathbf{r})$. The symmetry of the Coulomb integral $C_{ijkl}=C_{jilk}$ reduces the number of needed matrix elements to a half. For the single dot, ψ_i are the Fock-Darwin functions and it is possible to derive an analytical formula for C_{ijkl}. In our case, since the single-particle functions are given numerically, we have performed a numerical integration. Using the Fourier transform, we can reduce the four-dimensional integration to two dimensional

$$C_{ijkl}=2\pi\frac{e^2}{4\pi\epsilon_0\epsilon_r}\int d\mathbf{q}\tilde{\mathcal{F}}_{ik}(\mathbf{q})\tilde{\mathcal{F}}_{jl}(-\mathbf{q})\frac{1}{|\mathbf{q}|}, \tag{A8}$$

where

$$\tilde{\mathcal{F}}_{ik}(\mathbf{q})=\frac{1}{2\pi}\int d\mathbf{r}\mathcal{F}_{ik}(\mathbf{r})\exp(i\mathbf{q}\cdot\mathbf{r}). \tag{A9}$$

For the evaluation of the Fourier transforms, we use the Discrete Fourier transform algorithm with the attenuation factors, as described in Ref. 74.

We compute Eq. (A8) according to the perturbative formula

$$C_{ijkl}=\sum_{n,m}^{N_x,N_y}\sum_{k_1,k_2=0}^{k_1+k_2\le N}\sum_{l_1,l_2=0}^{k_1,k_2} I(l_1,l_2,n,m)\times\frac{(-q_n)^{(k_1-l_1)}}{(k_1-l_1)!l_1!}\frac{(-q_m)^{(k_2-l_2)}}{(k_2-l_2)!l_2!}\partial_x^{k_1}\partial_y^{k_2}f(\mathbf{q})|_{q_{nm}}, \tag{A10}$$

where $f(\mathbf{q})|_{q_{nm}}=\tilde{\mathcal{F}}_{ik}(\mathbf{q})\tilde{\mathcal{F}}_{jl}(-\mathbf{q})$ is calculated in the point q_{nm}, N is the perturbative order (the order of the Taylor expansion), N_x and N_y are the number of grid points in the x and y directions, respectively. The coefficients $I(l_1,l_2,n,m)$ depend only on the geometry of the grid and are defined as

$$I(l_1,l_2,n,m)=\int_{\Omega_x}dx\int_{\Omega_y}dy\frac{x^{l_1}y^{l_2}}{\sqrt{x^2+y^2}}. \tag{A11}$$

Here $\Omega_x=\langle(n-1/2)\delta_x,(n+1/2)\delta_x\rangle$ is the integration region and δ_x is the grid spacing along x. Similarly for the y direction. In our simulations we use the previous formula up to the fourth order in the Taylor expansion. The achieved relative precision is 10^{-5}, with the computational time for one Coulomb element ≈50 ms.

APPENDIX B: TWO-ELECTRON SYMMETRY

Suppose the single-particle Hamiltonian commutes with certain set of operators $\{O_\alpha\}$, and therefore the single-particle states ψ_i can be chosen such that they have definite symmetries forming a representation of the group O of the symmetry operators

$$O_\alpha\psi_i=o_\alpha^i\psi_i. \tag{B1}$$

For example, since the double-dot potential has inversion symmetry along x axis, I_x is in the group O while $o_x^i=\pm1$—the states are symmetric or antisymmetric with respect to x inversion. Now consider the two-electron states $|\Psi_{s/t}^{(i,j)}\rangle$, Eqs. (A1)–(A3). These states also have definite symmetry if a certain operator from O acts simultaneously on both particles

$$O_{\alpha,1}O_{\alpha,2}\Psi_{ij}=o_\alpha^i o_\alpha^j\Psi_{ij}. \tag{B2}$$

For our case of the symmetry group C_{2v}, since $o_\alpha^i=\pm1$, the set of all possible products of two characters is the same as the set of characters for a single particle, $\{o_\alpha^i o_\alpha^j\}_{i,j}=\{o_\alpha^i\}_i$. This means the two-particle states will form the same symmetry classes as single-particle states with the same characters.

APPENDIX C: HEITLER-LONDON APPROXIMATION

In the Heitler-London approximation, the exchange energy is calculated as

$$J_{HL}=\langle\Psi_-|H_{orb}|\Psi_-\rangle-\langle\Psi_+|H_{orb}|\Psi_+\rangle \tag{C1}$$

with the functions $\Psi_\pm$ given in Eq. (39). The single-particle ground-state wave function of the Fock-Darwin spectrum is

$$\psi_{00}(x,y)=\frac{1}{l_B\sqrt{\pi}}\exp\left[-\frac{x^2+y^2}{2l_B^2}\right], \tag{C2}$$

where l_B is the effective confinement length defined by $l_B^2=l_0^2/\sqrt{1+B^2e^2l_0^4/4\hbar^2}$. The wave functions $\psi_{L(R)}$ are obtained shifting the Fock-Darwin ground state to $(\pm l_0 d,0)$. In the presence of the magnetic field we have to add a phase factor because of the gauge transformation $\vec{A}'=B/2(-y,x\pm d)\rightarrow\vec{A}=B/2(-y,x)$; we have

$$\psi_{L(R)}=\exp\left[\pm id\zeta\vartheta\frac{y}{l_0}\right]\psi_{00}(x\pm l_0 d,y),$$

$$\zeta=\left(\frac{l_0}{l_B}\right)^2,\quad \vartheta=\frac{Bel_B^2}{2\hbar},\quad l_B=l_0(1-\vartheta^2)^{1/4}. \tag{C3}$$

The overlap between the left and right functions is

$$\Omega=\langle\psi_L|\psi_R\rangle=\exp[-\zeta d^2(1+\vartheta^2)] \tag{C4}$$

and the exchange energy is

$$J_{HL} = \frac{\hbar\omega_0}{\sinh[2\zeta d^2(1+\vartheta^2)]}\Bigg\{ c_s\sqrt{\zeta}[\exp[-\zeta d^2]I_0(\zeta d^2) + -\exp[\zeta d^2\vartheta^2]I_0(\zeta d^2\vartheta^2)] + \frac{2d}{\sqrt{\pi\zeta}}[1-\exp(-\zeta d^2)] + 2d^2[1-\mathrm{erf}(d\sqrt{\zeta})]\Bigg\}, \tag{C5}$$

where I_0 is the zeroth-order modified Bessel function of the first kind. The factor c_s is the ratio between the Coulomb strength and the confinement energy, $c_s = e^2\sqrt{\pi/2}/4\pi\varepsilon_0\varepsilon_r l_0\hbar\omega_0$. Similar formula can be found in Ref. 75 for a quartic confinement potential. Formula (C5) has been derived in Ref. 15 (in the original paper there is a trivial typo that we correct).

The two-electron energies for the states Ψ_- and Ψ_+ are

$$E_\pm = 2\hbar\omega_0\zeta + \frac{E_{RI}+E_{W_{RI}} \pm (E_{CE}+E_{W_{CE}})}{1\pm\Omega^2}, \tag{C6}$$

where

$$E_{RI} = \hbar\omega_0 c_s\sqrt{\zeta}\,\exp[-\zeta d^2]I_0(\zeta d^2),$$

$$E_{W_{RI}} = \hbar\omega_0\left\{2d^2[1-\mathrm{erf}(d\sqrt{\zeta})] - \frac{2d}{\sqrt{\zeta\pi}}\exp[-\zeta d^2]\right\},$$

$$E_{CE} = \hbar\omega_0 c_s\sqrt{\zeta}\,\exp[-\zeta d^2(2+\vartheta^2)]I_0(\zeta d^2\vartheta^2),$$

$$E_{W_{CE}} = -\hbar\omega_0\frac{2d}{\sqrt{\pi\zeta}}\exp[-2\zeta d^2(1+\vartheta^2)].$$

The components of the vectors $\mathbf{a}'$ and $\mathbf{b}'$ are

$$a'_x = 0, \quad a'_y = 0, \tag{C7}$$

$$b'_x = -\frac{\hbar^2}{2ml_d}\frac{\Omega^2}{\sqrt{1-\Omega^4}}\frac{\zeta d}{l_0}(1-\vartheta^2), \tag{C8}$$

$$b'_y = -\frac{\hbar^2}{2ml_{br}}\frac{\Omega^2}{\sqrt{1-\Omega^4}}\frac{\zeta d}{l_0}(1-\vartheta^2). \tag{C9}$$

where l_{br} and l_d are the spin-orbit lengths for the Rashba and Dresselhaus, respectively.

The matrix elements of the vector $\mathbf{n}$ are

$$\langle\Psi_+|n_{x,1}|\Psi_-\rangle = -\frac{dl_0}{\sqrt{1-\Omega^4}}\left(\frac{1}{l_d} + i\Omega^2\frac{\vartheta}{l_{br}}\right), \tag{C10}$$

$$\langle\Psi_+|n_{y,1}|\Psi_-\rangle = -\frac{dl_0}{\sqrt{1-\Omega^4}}\left(\frac{1}{l_{br}} + i\Omega^2\frac{\vartheta}{l_d}\right), \tag{C11}$$

and

$$\mu B_{so} = \frac{K_-}{1-\Omega^2}\vartheta[1-\Omega^2(1-\zeta d-\zeta d^2\vartheta^2)]. \tag{C12}$$

APPENDIX D: SPIN MATRICES

In the singlet and triplet basis, one can evaluate the 16 matrices which can be formed as the direct product of two Pauli matrices and the identity. Here we list only the matrices needed for our purposes, and we regroup them to combinations in which they appear in the text,

$$\boldsymbol{\sigma}_1\cdot\boldsymbol{\sigma}_2 = \begin{pmatrix} -3 & 0 & 0 & 0 \\ 0 & 1 & 0 & 0 \\ 0 & 0 & 1 & 0 \\ 0 & 0 & 0 & 1 \end{pmatrix}, \tag{D1}$$

$$\boldsymbol{\sigma}_1-\boldsymbol{\sigma}_2 = \left\{\begin{pmatrix} 0 & 0 & -\sqrt{2} & \sqrt{2} \\ 0 & 0 & 0 & 0 \\ -\sqrt{2} & 0 & 0 & 0 \\ \sqrt{2} & 0 & 0 & 0 \end{pmatrix}, \begin{pmatrix} 0 & 0 & -\sqrt{2}i & -\sqrt{2}i \\ 0 & 0 & 0 & 0 \\ \sqrt{2}i & 0 & 0 & 0 \\ \sqrt{2}i & 0 & 0 & 0 \end{pmatrix}, \begin{pmatrix} 0 & 2 & 0 & 0 \\ 2 & 0 & 0 & 0 \\ 0 & 0 & 0 & 0 \\ 0 & 0 & 0 & 0 \end{pmatrix}\right\}, \tag{D2}$$

$$\boldsymbol{\sigma}_1\times\boldsymbol{\sigma}_2 = \left\{\begin{pmatrix} 0 & 0 & -\sqrt{2}i & \sqrt{2}i \\ 0 & 0 & 0 & 0 \\ \sqrt{2}i & 0 & 0 & 0 \\ -\sqrt{2}i & 0 & 0 & 0 \end{pmatrix}, \begin{pmatrix} 0 & 0 & \sqrt{2} & \sqrt{2} \\ 0 & 0 & 0 & 0 \\ \sqrt{2} & 0 & 0 & 0 \\ \sqrt{2} & 0 & 0 & 0 \end{pmatrix}, \begin{pmatrix} 0 & 2i & 0 & 0 \\ -2i & 0 & 0 & 0 \\ 0 & 0 & 0 & 0 \\ 0 & 0 & 0 & 0 \end{pmatrix}\right\}, \tag{D3}$$

$$\boldsymbol{\sigma}_1 + \boldsymbol{\sigma}_2 = \left\{ \begin{pmatrix} 0 & 0 & 0 & 0 \\ 0 & 0 & \sqrt{2} & \sqrt{2} \\ 0 & \sqrt{2} & 0 & 0 \\ 0 & \sqrt{2} & 0 & 0 \end{pmatrix}, \begin{pmatrix} 0 & 0 & 0 & 0 \\ 0 & 0 & \sqrt{2}i & -\sqrt{2}i \\ 0 & -\sqrt{2}i & 0 & 0 \\ 0 & \sqrt{2}i & 0 & 0 \end{pmatrix}, \begin{pmatrix} 0 & 0 & 0 & 0 \\ 0 & 0 & 0 & 0 \\ 0 & 0 & 2 & 0 \\ 0 & 0 & 0 & -2 \end{pmatrix} \right\}. \tag{D4}$$

[1] E. Lieb and D. Mattis, Phys. Rev. **125**, 164 (1962).
[2] R. Hanson, L. P. Kouwenhoven, J. R. Petta, S. Tarucha, and L. M. K. Vandersypen, Rev. Mod. Phys. **79**, 1217 (2007).
[3] D. Loss and D. P. DiVincenzo, Phys. Rev. A **57**, 120 (1998).
[4] X. Hu and S. Das Sarma, Phys. Rev. A **61**, 062301 (2000).
[5] K. C. Nowack, F. H. L. Koppens, Y. V. Nazarov, and L. M. K. Vandersypen, Science **318**, 1430 (2007).
[6] F. H. L. Koppens, C. Buizert, K. J. Tielrooij, I. T. Vink, K. C. Nowack, T. Meunier, L. P. Kouwenhoven, and L. M. K. Vandersypen, Nature (London) **442**, 766 (2006).
[7] J. R. Petta, A. C. Johnson, J. M. Taylor, E. A. Laird, A. Yacoby, M. D. Lukin, C. M. Marcus, M. P. Hanson, and A. C. Gossard, Science **309**, 2180 (2005).
[8] W. A. Coish and D. Loss, Phys. Rev. B **75**, 161302 (2007).
[9] V. Popsueva, R. Nepstad, T. Birkeland, M. Førre, J. P. Hansen, E. Lindroth, and E. Waltersson, Phys. Rev. B **76**, 035303 (2007).
[10] E. A. Laird, J. R. Petta, A. C. Johnson, C. M. Marcus, A. Yacoby, M. P. Hanson, and A. C. Gossard, Phys. Rev. Lett. **97**, 056801 (2006).
[11] G. Burkard, G. Seelig, and D. Loss, Phys. Rev. B **62**, 2581 (2000).
[12] U. Merkt, J. Huser, and M. Wagner, Phys. Rev. B **43**, 7320 (1991).
[13] R. de Sousa, X. Hu, and S. Das Sarma, Phys. Rev. A **64**, 042307 (2001).
[14] W. Dybalski and P. Hawrylak, Phys. Rev. B **72**, 205432 (2005).
[15] J. Pedersen, C. Flindt, N. A. Mortensen, and A.-P. Jauho, Phys. Rev. B **76**, 125323 (2007).
[16] J. I. Climente, A. Bertoni, G. Goldoni, M. Rontani, and E. Molinari, Phys. Rev. B **75**, 081303 (2007).
[17] L. P. Gor'kov and P. L. Krotkov, Phys. Rev. B **68**, 155206 (2003).
[18] D. V. Melnikov, J.-P. Leburton, A. Taha, and N. Sobh, Phys. Rev. B **74**, 041309 (2006).
[19] T. Q. Nguyen, Mary Clare Sison Escaño, N. Shimoji, H. Nakanishi, and H. Kasai, Phys. Rev. B **77**, 195307 (2008).
[20] B. S. Kandemir, Phys. Rev. B **72**, 165350 (2005).
[21] D. Pfannkuche, V. Gudmundsson, and P. A. Maksym, Phys. Rev. B **47**, 2244 (1993).
[22] C. Yannouleas and U. Landman, Phys. Rev. B **68**, 035325 (2003).
[23] C. Yannouleas and U. Landman, Int. J. Quantum Chem. **90**, 699 (2002).
[24] L. Serra, R. G. Nazmitdinov, and A. Puente, Phys. Rev. B **68**, 035341 (2003).
[25] H. Saarikoski, E. Räsänen, S. Siljamäki, A. Harju, M. J. Puska, and R. M. Nieminen, Eur. Phys. J. B **26**, 241 (2002).
[26] L. He, G. Bester, and A. Zunger, Phys. Rev. B **72**, 195307 (2005).
[27] I. Žutić, J. Fabian, and S. Das Sarma, Rev. Mod. Phys. **76**, 323 (2004).
[28] J. Fabian, A. Matos-Abiague, C. Ertler, P. Stano, and I. Žutić, Acta Phys. Slov. **57**, 565 (2007).
[29] P. Stano and J. Fabian, Phys. Rev. Lett. **96**, 186602 (2006).
[30] Y. G. Semenov and K. W. Kim, Phys. Rev. B **75**, 195342 (2007).
[31] T. Meunier, I. T. Vink, L. H. Willems van Beveren, K.-J. Tielrooij, R. Hanson, F. H. L. Koppens, H. P. Tranitz, W. Wegscheider, L. P. Kouwenhoven, and L. M. K. Vandersypen, Phys. Rev. Lett. **98**, 126601 (2007).
[32] S. Sasaki, T. Fujisawa, T. Hayashi, and Y. Hirayama, Phys. Rev. Lett. **95**, 056803 (2005).
[33] S. C. Badescu, Y. B. Lyanda-Geller, and T. L. Reinecke, Phys. Rev. B **72**, 161304 (2005).
[34] J. H. Jiang, Y. Y. Wang, and M. W. Wu, Phys. Rev. B **77**, 035323 (2008).
[35] J. L. Cheng, M. W. Wu, and C. Lü, Phys. Rev. B **69**, 115318 (2004).
[36] K. Shen and M. W. Wu, Phys. Rev. B **76**, 235313 (2007).
[37] J. I. Climente, A. Bertoni, G. Goldoni, M. Rontani, and E. Molinari, Physica E **40**, 1804 (2008).
[38] L. Meza-Montes, C. F. Destefani, and S. E. Ulloa, Phys. Rev. B **78**, 205307 (2008).
[39] A. Pfund, I. Shorubalko, K. Ensslin, and R. Leturcq, Phys. Rev. B **79**, 121306 (2009).
[40] D. V. Khomitsky and E. Y. Sherman, Phys. Rev. B **79**, 245321 (2009).
[41] P. Stano and J. Fabian, Phys. Rev. B **77**, 045310 (2008).
[42] D. V. Khomitsky and E. Ya. Sherman, Europhys. Lett. **90**, 27010 (2010).
[43] P. San-Jose, B. Scharfenberger, G. Schön, A. Shnirman, and G. Zarand, Phys. Rev. B **77**, 045305 (2008).
[44] H. Imamura, P. Bruno, and Y. Utsumi, Phys. Rev. B **69**, 121303 (2004).
[45] M. Yang and S.-S. Li, Phys. Rev. B **74**, 073402 (2006).
[46] M. M. Glazov and V. D. Kulakovskii, Phys. Rev. B **79**, 195305 (2009).
[47] S. J. Devitt, J. H. Cole, and L. C. L. Hollenberg, Phys. Rev. A **73**, 052317 (2006).
[48] S. Chutia, M. Friesen, and R. Joynt, Phys. Rev. B **73**, 241304 (2006).
[49] N. Zhao, L. Zhong, J.-L. Zhu, and C. P. Sun, Phys. Rev. B **74**, 075307 (2006).
[50] D. Stepanenko and N. E. Bonesteel, Phys. Rev. Lett. **93**, 140501 (2004).
[51] N. E. Bonesteel, D. Stepanenko, and D. P. DiVincenzo, Phys. Rev. Lett. **87**, 207901 (2001).
[52] G. Burkard and D. Loss, Phys. Rev. Lett. **88**, 047903 (2002).
[53] L.-A. Wu and D. A. Lidar, Phys. Rev. A **66**, 062314 (2002).

[54] T. Moriya, Phys. Rev. **120**, 91 (1960).
[55] I. Dzyaloshinsky, J. Phys. Chem. Solids **4**, 241 (1958).
[56] S. Gangadharaiah, J. Sun, and O. A. Starykh, Phys. Rev. Lett. **100**, 156402 (2008).
[57] L. Shekhtman, O. Entin-Wohlman, and A. Aharony, Phys. Rev. Lett. **69**, 836 (1992).
[58] A. Zheludev, S. Maslov, G. Shirane, I. Tsukada, T. Masuda, K. Uchinokura, I. Zaliznyak, R. Erwin, and L. P. Regnault, Phys. Rev. B **59**, 11432 (1999).
[59] K. V. Kavokin, Phys. Rev. B **64**, 075305 (2001).
[60] K. V. Kavokin, Phys. Rev. B **69**, 075302 (2004).
[61] L. P. Gor'kov and P. L. Krotkov, Phys. Rev. B **67**, 033203 (2003).
[62] L. S. Levitov and E. I. Rashba, Phys. Rev. B **67**, 115324 (2003).
[63] F. Baruffa, P. Stano, and J. Fabian, Phys. Rev. Lett. **104**, 126401 (2010).
[64] C. Herring, Rev. Mod. Phys. **34**, 631 (1962).
[65] P. Lucignano, B. Jouault, and A. Tagliacozzo, Phys. Rev. B **69**, 045314 (2004).
[66] M. Rontani, F. Troiani, U. Hohenester, and E. Molinari, Solid State Commun. **119**, 309 (2001).
[67] P. Stano and J. Fabian, Phys. Rev. B **72**, 155410 (2005).
[68] J. M. Elzerman, R. Hanson, L. H. Willems van Beveren, B. Witkamp, L. M. K. Vandersypen, and L. P. Kouwenhoven, Nature (London) **430**, 431 (2004).
[69] I. L. Aleiner and V. I. Fal'ko, Phys. Rev. Lett. **87**, 256801 (2001).
[70] J. Fabian and S. Das Sarma, Phys. Rev. Lett. **81**, 5624 (1998).
[71] O. Olendski and T. V. Shahbazyan, Phys. Rev. B **75**, 041306 (2007).
[72] S. Takahashi, R. S. Deacon, K. Yoshida, A. Oiwa, K. Shibata, K. Hirakawa, Y. Tokura, and S. Tarucha, Phys. Rev. Lett. **104**, 246801 (2010).
[73] H. E. Türeci and Y. Alhassid, Phys. Rev. B **74**, 165333 (2006).
[74] W. H. Press, S. A. Teukolsky, W. T. Vetterling, and B. P. Flannery, *Numerical Recipes: The Art of Scientific Computing*, 3rd ed. (Cambridge University Press, Cambridge, England, 2007).
[75] G. Burkard, D. Loss, and D. P. DiVincenzo, Phys. Rev. B **59**, 2070 (1999).